REPORT DOCUMENTATION PAGE

Form Approved
OMB No. 0704-0188

1. REPORT DATE *(DD-MM-YYYY)*	**2. REPORT TYPE**	**3. DATES COVERED** *(From - To)*
15-03-2012	Technical Paper	

4. TITLE AND SUBTITLE

Spray Statistics and the Impact of Geometry in Gas-Centered Swirl Coaxial Injectors

5a. CONTRACT NUMBER

5b. GRANT NUMBER

5c. PROGRAM ELEMENT NUMBER

6. AUTHOR(S)
Malissa D.A. Lightfoot, Alan L. Kastengren, S. Alexander Schumaker, and Stephen A. Danczyk

5d. PROJECT NUMBER

5f. WORK UNIT NUMBER
50260538

7. PERFORMING ORGANIZATION NAME(S) AND ADDRESS(ES)

Air Force Research Laboratory (AFMC)
AFRL/RZSA
10 E. Saturn Blvd.
Edwards AFB CA 93524-7680

8. PERFORMING ORGANIZATION REPORT NUMBER

9. SPONSORING / MONITORING AGENCY NAME(S) AND ADDRESS(ES)

Air Force Research Laboratory (AFMC)
AFRL/RZS
5 Pollux Drive
Edwards AFB CA 93524-7048

10. SPONSOR/MONITOR'S ACRONYM(S)

11. SPONSOR/MONITOR'S NUMBER(S)
AFRL-RZ-ED-TP-2012-078

12. DISTRIBUTION / AVAILABILITY STATEMENT

Approved for public release; distribution unlimited (PA #12230).

13. SUPPLEMENTARY NOTES
For presentation at the 24th Annual Conference on Liquid Atomization and Spray Systems (ILASS-Americas), San Antonio, TX, 20-23 May 2012.

14. ABSTRACT

Optically dense sprays are often encountered in propulsion applications such as rocket engines. The density of these sprays prevents measurement of droplet diameters and quantitative assessment of spray quality. The lack of quantitative data hinders the development of design criteria and complicates the formation of a fundamental understanding of the impact changes to injector geometry make in an engine's performance. While recent strides have been made in attaining qualitative data on a particular injector—a Gas-Centered Swirl Coaxial injector—with a very dense spray, droplet measurements and spray statistics have remained elusive. The current work presents the first of such quantitative measurements—measurements achieved using time-resolved x-ray radiography. Details are given on a new experimental set-up used to produce relevant flow conditions at Argonne National Laboratory's Advanced Photon Source and the data processing used to extract droplet diameters and velocities. These extracted data are then used to assess how changes in the geometry of a GCSC injector alter the spray. Changes in liquid inlet diameter and liquid swirl number are shown to impact the spray in unexpected ways. The effect of injector outlet diameter changes and the downstream evolution of the spray are also discussed.

15. SUBJECT TERMS

16. SECURITY CLASSIFICATION OF:			**17. LIMITATION OF ABSTRACT**	**18. NUMBER OF PAGES**	**19a. NAME OF RESPONSIBLE PERSON**
					Dr. Malissa D.A. Lightfoot
a. REPORT	**b. ABSTRACT**	**c. THIS PAGE**			**19b. TELEPHONE NUMBER** *(include area code)*
Unclassified	**Unclassified**	**Unclassified**	SAR	17	N/A

Spray Statistics and the Impact of Geometry in Gas-Centered Swirl Coaxial Injectors

Malissa D.A. Lightfoot[1*], Alan L. Kastengren[2], S. Alexander Schumaker[1], Stephen A. Danczyk[1]
[1]Air Force Research Laboratory, Edwards AFB, CA
[2]Argonne National Laboratory, Argonne, IL

Abstract

Optically dense sprays are often encountered in propulsion applications such as rocket engines. The density of these sprays prevents measurement of droplet diameters and quantitative assessment of spray quality. The lack of quantitative data hinders the development of design criteria and complicates the formation of a fundamental understanding of the impact changes to injector geometry make in an engine's performance. While recent strides have been made in attaining qualitative data on a particular injector—a Gas-Centered Swirl Coaxial injector—with a very dense spray, droplet measurements and spray statistics have remained elusive. The current work presents the first of such quantitative measurements—measurements achieved using time-resolved x-ray radiography. Details are given on a new experimental set-up used to produce relevant flow conditions at Argonne National Laboratory's Advanced Photon Source and the data processing used to extract droplet diameters and velocities. These extracted data are then used to assess how changes in the geometry of a GCSC injector alter the spray. Changes in liquid inlet diameter and liquid swirl number are shown to impact the spray in unexpected ways. The effect of injector outlet diameter changes and the downstream evolution of the spray are also discussed.

[*]Corresponding author: malissa.lightfoot@edwards.af.mil

Introduction

Increasing the performance of a rocket while decreasing launch and development costs requires a strong understanding of all the components of the engine. For the injector component, the important characteristics are the atomization and mixing performance. A well-developed set of design criteria for an injector can greatly reduce engine development costs [1]. However, the hostile environment and complexity of a rocket engine make the development of such criteria challenging. As a result, simplifications are made including scaling to allow testing without combustion and the examination of a single (versus an array of) element.

Design criteria development and testing requires extensive knowledge of the spray, particularly in the primary atomization and near-injector zones. Unfortunately, despite the above-listed simplifications, measurements in these regions remain elusive. Semi-quantitative assessments using techniques such as shadowgraphy and ballistic imaging plus a physical understanding of the likely processes involved can lead to basic scaling laws. Such a set of basic design criteria has been developed over the last several years for Gas-Centered Swirl Coaxial (GCSC) injectors [2].

GCSC injectors are of interest in the atomization of hydrocarbon fuels when gaseous oxidizer is available at the injector. This particular type of prefilming atomizer involves a swirling, annular flow with a nonswirled axial gas flow down the center of the injector. Prior assessments, based on cold flow studies mainly employing shadowgraphy and other imaging techniques, have determined that momentum flux ratio is the main scaling parameter for atomization efficiency [2]. From examination of the liquid film behavior, swirl appears to have minimal effect on the injector performance [2, 3]. However, shadowgraphy of the spray and images of the film profile provide only limited data with no information on droplet size, velocity and their distributions.

The size, velocity and number of droplets at various locations in a spray are key parameters for understanding the atomization process and effectiveness of an atomizer. Numerous laser diagnostics exist to provide these data as well as the overall mass distribution of a spray. Using these diagnostics on optically dense sprays is either impossible or involves the use of techniques to reduce the optical density, such as scaling, inference from downstream measurements or spray splitting. These techniques are complex to implement and questions arise regarding how they alter the spray. In recent years ballistic imaging have been able to provide qualitative information [4], and more traditional techniques, such as patternation, have been able to provide limited quantitative time-averaged information [5]. These diagnostics continue to struggle in the near-exit region of the spray and quantitative information on droplet size and velocity in any location within dense sprays has remained elusive. X-ray radiography has the promise of providing these details in sprays whose optical densities prevent the use of conventional laser diagnostics.

X-ray radiography has received much attention as a spray diagnostic in recent years [6-10]. Much of this work has focused on mass flux and/or mass distribution of the spray, with time-resolved methods able to provide the spray evolution of diesels sprays [9, 10]. In situations where the flow rates are steady, however, the time-resolved radiography offers the promise of providing discrete information about the amount of liquid within the line-of-sight of the x-ray beam at a given instance in time. GCSC injectors are believed to undergo the majority of their atomization within the cup of the injector, so that in the spray, i.e. downstream of the injector exit, only droplets or discrete “blobs” of liquid exist. X-ray radiography, then, should be able to give statistics on the droplet size and velocity in these dense sprays where other droplet-measuring diagnostics have failed.

Time-resolved x-ray radiographic studies of GCSC injectors have been conducted at Argonne National Laboratory’s Advanced Photon Source as part of a larger program studying the use of x-ray radiography in dense sprays. The time-resolved studies were not the main emphasis of the current program; however, simple analysis methods have been applied to the collected, time-resolved data. These simple methods require numerous assumptions but do provide some droplet statistics which can be used to learn how alterations in the geometry of the injector affect the spray and how the spray evolves in the near-injector region downstream of the exit. The methods of processing the time-resolved x-ray radiography data along with the limitations of the current analysis are given. Ways to overcome these limitations have been identified. The measured droplet sizes, velocities and some additional spray statistics are considered for individual sprays as a means to examine the performance of the diagnostic and the basic data-processing technique. Finally, the impact of downstream distance and changes in the GCSC geometry are explored through the developed spray statistics.

Experimental Methods

Hardware

These experiments were conducted at Argonne National Laboratory’s Advanced Photon Source (APS) in beamline 7-BM. This location has been conducting x-ray radiographic studies of sprays for several years [9-11]. The x-rays are produced by a synchrotron bending magnet and, as such, the raw (white beam)

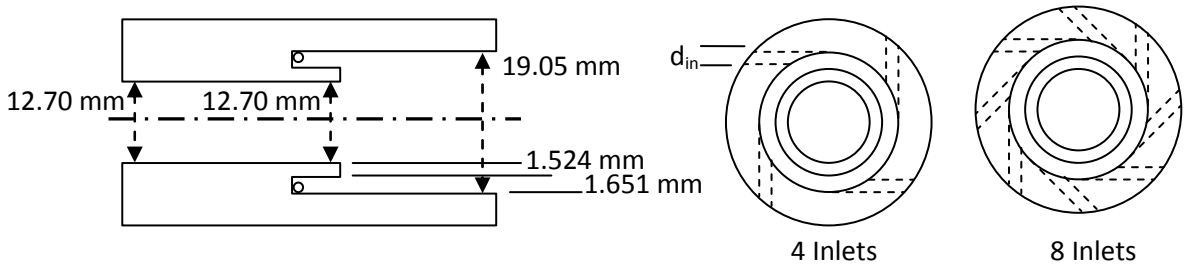

Figure 1: The nominal geometric cross-section of the GCSC injector is shown along with two different inlet configurations.

Case	Inlet #	Inlet Diameter	Gas Mass Flow	Liquid Mass Flow	Momentum Flux Ratio	R_A
4H	4	1.60 mm	46 g/s	30 g/s	88	0.30
8SA	8	0.99 mm	45 g/s	26 g/s	89	0.26
8DA	8	1.60 mm	46 g/s	40 g/s	88	0.41
OS	4	1.60 mm	45 g/s	35 g/s	86	0.32

Table 1: The flow conditions and geometry variations tested here. The OS case has a smaller outlet and gas-post diameter as noted in the text. R_A is the axial-to-total liquid velocity, an inverse indication of swirl level.

radiation is polychromatic and nearly collimated. Prior to use in radiographic studies, the beam is conditioned using a monochromator to create a monochromatic beam ($\Delta E/E$=1.4%). The beam is then focused to create a beam 5 by 6 μm FWHM (full width half maximum) at its narrowest point with 10 keV of photon energy. Additional details of this x-ray radiography set-up can be found in Ref. [11].

The experiments use a titanium foil and a PIN diode as detectors. The titanium foil detector uses the x-ray fluorescence from a thin (0.5 μm) sheet of titanium placed in the x-ray beam to monitor the incident x-ray intensity on the experiment. The PIN diode measures the intensity after the beam has traveled through the spray. Data was collected at 1 MHz and the signal was conditioned with a second-order low pass filter with a -3dB frequency of 300 kHz. Eight seconds of data was collected, but only 5 seconds of data is analyzed here (see the Results and Discussion section for more details). Thirty-three data points spaced 1 mm apart were taken across the spray width, i.e. perpendicular to the injector axis. These 33 measurements were made 3 mm from the injector face and again 5 mm from the injector face. A programmable linear translation stage was used to accurately position the spray relative to the fixed beam.

The spray was produced by a GCSC injector (Fig. 1). This type of injector produces a swirling, annular liquid film by introducing liquid through inlets drilled tangential to the injector cup. Nonswirling gas enters along the axis of the injector and atomizes the liquid, typically prior to the end of the injector. Three different inlet geometries were examined—two with 8 inlets and one with 4 inlets, as show in Fig. 1. The additional geometric parameters are listed in the figure. One case with a smaller outlet diameter was also examined. This geometry has 4 liquid inlets, the outlet diameter is 13.24 mm and the gas-post diameter just prior to liquid contact is 8.89 mm; the other geometric parameters remain unchanged.

This injector was originally designed to operate with liquid hydrocarbon and gaseous oxygen. In the interest of safety and simplicity, the cold-flow experiments have been performed using demineralized water and gaseous nitrogen. A special, mobile flow facility (MFL) was constructed by the Air Force Research Laboratory and transported to the APS for the testing. The MFL is a self-contained system with its own Pacific Instruments 6000 series data acquisition system and CompactLogix control system allowing the entire system to be run remotely. Liquid nitrogen, electrical power and an exhaust system are all that is required of the host facility. Gaseous nitrogen is produced by using a cryopump to increase the pressure of liquid nitrogen, supplied from either a drop or Dewar, to 408 atm. The high-pressure liquid nitrogen is then vaporized using a 24 kW electric vaporizer. Gaseous nitrogen is stored in two, 57-liter gas bottles. The flow system is designed to allow both bottles to be used in a blow down configuration or to run from one bottle while the other bottle is being filled. The gaseous nitrogen is also used to pressurize a 57 liter water tank. The available water was sufficient to complete several measurements prior to refilling the tank, and it was possible to pause the data collection between measurement points to do so. The MFL is capable of delivering water and gaseous nitrogen on the order of 450 g/s at pressures in excess of 130 atm.

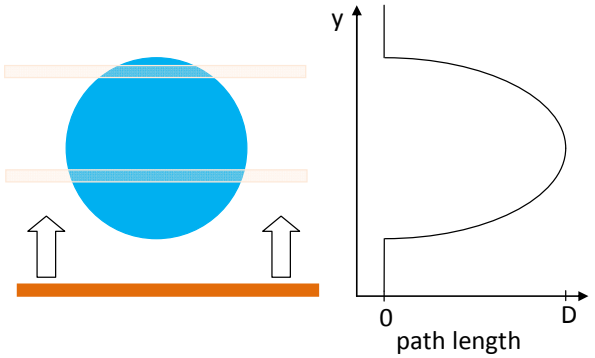

Figure 2: A single droplet moving through the beam creates a semi-elliptical profile.

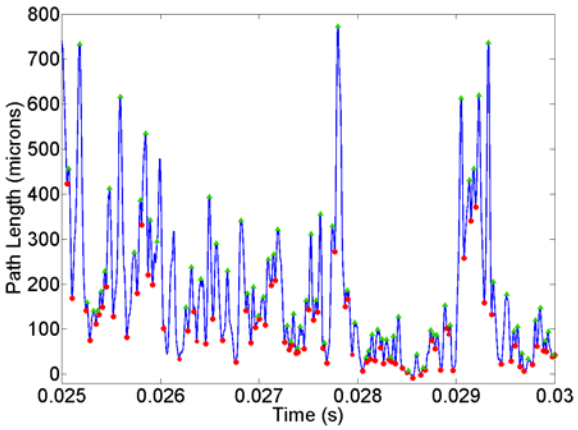

Figure 3: All peaks (green triangles) and troughs (red circles) found in a short time window are shown here.

Critical flow orifices were used to meter the gas and liquid flow rates with an uncertainty of approximately 4% and 0.5%, respectively. The nature of the beamline setup required an enclosed exhaust and vent system which differs from tests previously conducted using these injectors. The exhaust typically operated at <? ft3/s>. The limited space in the 7-BM hutch necessitated a curved exhaust duct. The distance from the spray to the back, curved surface was on the order of a meter. Because of the exhaust capabilities and to limit splash back of water (caused, in part, to the curved geometry of the outlet), gas flow rates were limited to ~46 g/s. The examined operating conditions are listed in Table 1.

Developing Droplet Statistics

Beer's law and the absorption coefficient of water [12] were used to convert the measured intensity to a path length of water through which the beam traveled. The titanium foil measurement was considered the incident intensity. Due to the time involved in downloading data along with the APS's basic operation, the incident intensity varied across measurement locations. There is little variation across a single, 8 second measurement. The PIN diode value was the measured intensity after traveling through the spray. The ratio of measured to incident intensity was further normalized by a baseline value before the logarithm was applied and the path length computed. The baseline value was taken to be the average value of the highest 1% of intensity values (PIN Diode/Titanium Foil).

A measure of the path length of water in the beam's line-of-sight is then available at every microsecond over an 8 second span. Because the current work is preliminary, only a 5 second subset of these data was processed. As will be detailed below, this subset still contains around 70,000 analyzed droplets at each measurement point. The average over this time series is the time-averaged path length reported in previous x-ray radiographic work [9].

When a droplet enters the beam there is an increase then decrease in the measured path length. A cartoon example of a single, spherical droplet moving through the beam is illustrated in Fig. 2. In this simple example it is clear that the maximum value of the measured path length, the value at the signal's peak, is equal to the diameter of the droplet and the time of the departure from zero can be used to calculate the droplet's velocity. The actual experiment contains a number of complications which make determining the diameter and velocity uncertain (which are detailed below). In general, though, the droplet diameters and velocities can be determined by examining the peaks and troughs (or beginning and end of flat areas between peaks—to simplify the text, "trough" will be used to designate the beginning and ending of an event which produces a peak). A Matlab routine was developed to find the location and values of the peaks and troughs in the time-resolved path lengths [13].

The signal contains some amount of noise; because this time-resolved process was not the focus of the study, the set-up was not optimized to minimize noise or maximize signal-to-noise ratio. To help ease the effect of this noise, the data were filtered using a running average prior to finding peaks and troughs. Here the running average is taken over 20 points. Levels from 5 to 50 points were considered. Filters from 10 to 30 points made little difference in the results. A 5 point filter found substantially more droplet events, which were of a level below what can be differentiated from noise, and a filter greater than 30 points had a decrease in the number of droplets found. Local peaks (and troughs) are found by looking for peaks (or their negatives) within a sliding window. The size of this window had only a slight effect on the peaks found. Several windows were tried, and a value of 20 points was selected from "by-eye" assessments of

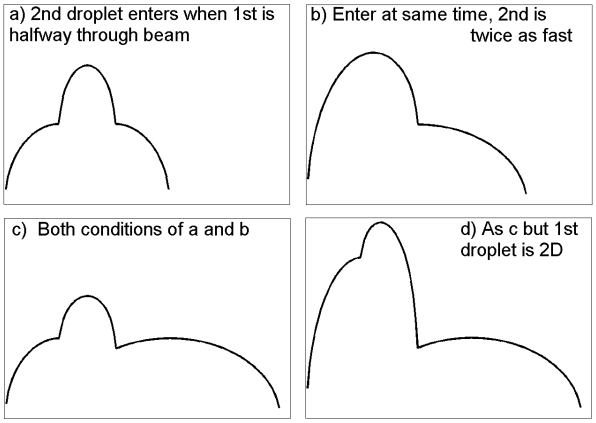

Figure 4: Two droplets which differ from each other create a complex time trace of the path length.

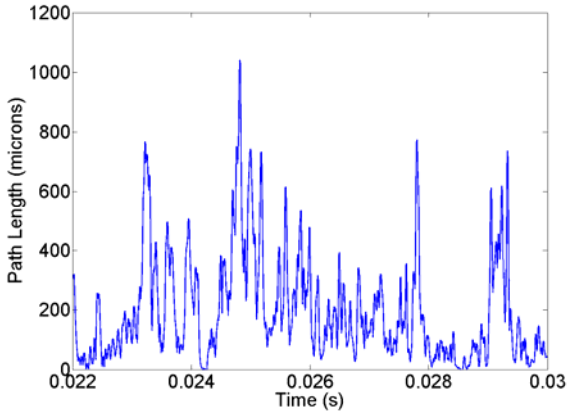

Figure 5: Large numbers of droplets are seen in this 5 ms window of the filtered data.

program performance. Once the peak and trough locations were found, the path length value at each of these locations and the time of each event (the distance between troughs on each side of a peak) was determined. The peak value was the maximum value between two troughs in the raw data. The trough values were an average over 5 points centered at the "found" location from the program. The trough values were averaged due to the noise, which has more impact on values near zero. Part of a typical, filtered time-resolved path length plot is shown in Fig. 3. The peaks and troughs found by the Matlab routine are marked.

Once the above data is extracted droplet diameters and velocities can be calculated. Here departures from the simple, single-droplet example considered above (Fig. 2) become important, particularly the likely scenario of multiple droplets existing within the line-of-sight probe volume. If two droplets enter at the same time and same speed, they will be viewed as a single, larger droplet with double the velocity. That scenario is rather unlikely, however, and if two droplets enter at different times or with different velocities they are discernable from each other. As the number of droplets increases, however, the ability to discern all droplets becomes less certain. Figure 4 contains some rough sketches of what time traces might look like with two different droplets entering. As would be expected from a high-optical-density spray, the path length data clearly show this multiple, overlapping peaks behavior (Fig. 3). In the long term, calibration and simulation experiments on known arrays of droplets (or hard spheres) should be conducted to fully understand these multiple-droplet effects. The current work, however, was not originally focused on the development of droplet measurements, so this fundamental groundwork has not yet been completed.

With multiple events stacked together determining the entering and/or leaving time for a droplet is difficult or impossible. Peak fitting of some type, as done in spectroscopy, might be used but is considered too complex for the current initial assessment. When multiple peaks exist, then, the elapsed time is the measured time between troughs, even if the path length does not start or return to zero. As a result, elapsed times are likely underestimated in many cases leading to an increase in calculated velocity. The droplet diameter is determined by subtracting the value at each trough bounding the peak from the peak value; the maximum difference is kept. An advantage of this procedure is that the results are essentially independent of changes or errors in the baseline value. If two droplets enter the beam at the same time but with different velocities the faster droplet will appear larger with the error being proportional to and decreasing with the velocity. The analysis would be able to measure the correct time to traverse the beam, but the error in diameter would cause this droplet's velocity to be bias upwards. The slower droplet, on the other hand, will have the droplet diameter measured correctly but the time in the beam with be decreased proportional to the velocity difference in the droplets. In another simple case with two droplets, their velocities are the same but they enter the beam at offset times. In this situation an erroneous third droplet is found by the automated program. The two "real" droplets are measured to be at or below their actual size with larger lag times leading to smaller measured diameters and less calculated in-beam time. The extra droplet is measured to be smaller and traverse through the beam more quickly as the shift increases. A combination of different velocities and lags between entering the measurement volume produce a combination of the two behaviors. As additional droplets enter at the same time, the relation to actual droplet diameter and velocity becomes more convoluted. If all droplets can be discerned then this procedure is inclined to underestimate some diameters and find extra droplets which are, in general, larger than the smallest real droplets. However, if not all of the

droplets have separate, discernable peaks then at least some of the diameters will be overestimated. Figure 5 shows an experimental case where several droplets enter and leave the beam throughout a period (see especially 0.03 to 0.0305 seconds). Note the overall bell-like shape underlying the series of peaks. This type of behavior clearly indicates that there are multiple droplets in the line-of-sight and suggests that some may not be resolved.

There are additional complications beyond the example case in Fig. 2 and the situation with multiple droplets simultaneously within the beam. The droplet may travel through the beam off-center so that a chord is measured instead of the diameter. This droplet will appear smaller than it actually is. Similarly, the data has a finite sampling rate which may not capture the maximum droplet diameter as the droplet travels through the probe. However, simple calculations show that a droplet which remains in the beam for 5 samples (5 μs) will result in a measured droplet diameter within 97% of the droplet's actual diameter. The droplet may not be traveling perpendicular to the beam resulting in a calculated velocity which is slower than it is actually traveling. An assumption has been made that droplets are spherical. Nonspherical droplets could create a bias in either direction depending on the orientation of the droplet with respect to the beam. The filtering, 20 points, and the temporal resolution (1 μs) create an upper threshold in the velocity that can be captured. This limit is a function of droplet size; droplets traveling faster than this limit are not resolved with the current data-processing technique. This limit is discussed in more detail below. The current data was acquired at a rate well below the maximum which can be achieved at APS's 7-BM and was set based on potential instability frequencies which might exist in the sprays under investigation rather than in an attempt to fully resolve droplets and their velocities. The signal noise also creates a lower threshold in droplet diameter which is discernable which is also discussed in detail below.

Herein, as above, the focus is on the arithmetic mean of the diameter, the D_{10} measurement, and diameter measurements in general. The radiography technique essentially measures an extinction of water within a beam of very small cross section (which is much smaller than the droplet cross section), so it measures the average length of water in the beam, overall a diameter, and not surface area or volume. Also, the possibility of overlapping droplets where droplet diameter is overestimated discourages the use of volume-weighted averages since the overestimation of diameter would strongly impact the D_{30} value. Similarly, distributions (histograms) are given in terms of the diameter and not in terms of Sauter Mean diameters or volumetric diameters. Distributions are typically given as probabilities—the number of droplets in a certain bin divided by the total number of droplets in the measurement. However, when probability density functions are discussed and shown, densities are used. Density normalizes the area under the distribution to one (i.e. divides by the bin size).

Results and Discussion

Statistics from Individual Conditions

Typically, the data processing program locates around 14,000 droplets in a 1 second measurement window. For the sprays examined here, the number of droplets found is essentially consistent in time (with no strong frequencies); in other words, the number of droplets scales more or less directly with measurement time. Figure 6 shows how the arithmetic mean diameter (D_{10}) and velocity change as a function of the number of droplets for case 8SA at the sprays' centerline both 3 and 5 mm from the injector exit. Even up to 5 seconds, where approximately 70,000 droplets have been recorded, some amount of variation remains in the droplet and velocity means of some cases. One of the major reasons for this is the sporadic measurement of very large droplets, typically greater than 2 mm. These may be the result of water accumulating and shedding from the face of the injector in the current configuration. However, vertically oriented shadowgraphy also shows occasional large droplets which do not seem to result from dripping off of the injector face. Regardless, one or occasionally two such events may occur in a 5 second period, and a sufficient number of droplets must be considered to be tolerant of such outlying points. These large droplets and the general distribution (nonnormal) of droplets preclude rigorous application of the central limit theorem to determine the number of droplets needed to achieve a converged mean with some known confidence level. An examination of the variance of the

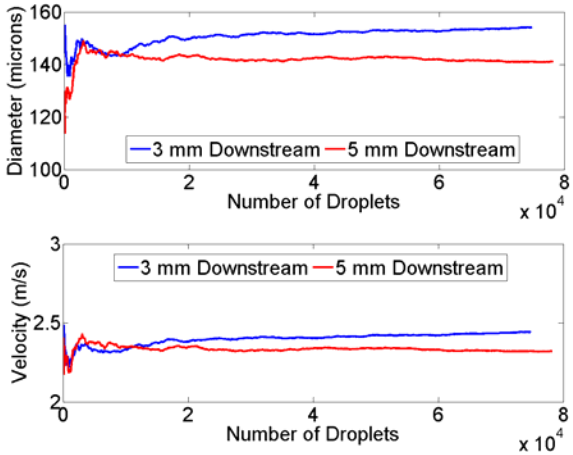

Figure 6: Behavior of the arithmetic means over an increasing number of droplets is shown for case 8SA.

mean as additional droplets are considered in the average was undertaken in an attempt to determine how many droplets are needed to produce converged means. In a worst case, 95% of the droplets within a 5 second window must be averaged to reach variations of less than 1% in the mean droplet diameter. Typically, though, averaging beyond 50-70% of the droplets in the 5 second window produces variation in the mean of less than 1%. A 5% or less variation in the mean requires a minimum of 3 to 15% of the droplets. Given the initial exploratory nature of this work and the time currently required to process data, a 5 second time window was chosen instead of using the entire available 8 seconds of data. The current results do not clearly indicate convergence of the means across all conditions and measurement locations. However, utilizing 5 seconds of data should provide means which are converged closer than 5% of their asymptotic values and, within the constraints and uncertainties of the current data analysis methods as discussed above, will provide reliable droplet statistics.

As discussed in the Experimental Methods section, all of the time-resolved path length data have a similar general character of peaks as illustrated in Fig. 3. This general character is even found in cases with no water flow and in measurement locations outside of the spray. However, in these cases where no droplets are present, the calculated droplet diameter is always in the range of tens of microns. Figure 7 shows a typical trace without water compared to one near the center of a spray. The scale does not allow the individual peaks and troughs of the data with no water flowing to be seen. (Only 4 seconds of data are available for the cases with no water.) Because a similar structure exists, the processing resolves droplets even though the lack of water flow guarantees no droplets are present. The mean droplet size (D_{10}) calculated from tests without water flowing was 23 microns and the 95th percentile droplet diameter (based on diameter not volume) was 35 microns. When water was flowing, the lack of droplets cannot be guaranteed, but there are measurement areas which are out of the main body of the spray. Because large droplets are occasionally measured throughout the 32 mm investigated width, the definition of "outside" the spray is not necessarily straightforward. However, there is generally an abrupt change in droplet diameter distributions which can be used to indicate the spray boundary (Fig.8). There are some cases where the changeover is less obvious; if no obvious transition was observed, none of the locations were considered for the current analysis determining noise levels. At locations whose diameter distributions clearly show they are outside the spray, noise levels were assessed considering only droplets below 500 microns. This level is relatively arbitrary but was set to be well beyond the peaks found with no water flowing. From these locations, there was a clear change in either the noise level or the amount of residual background mist remaining in the exhaust area during a test. Cases 4H and 8SA are similar and 8DA and OS are similar. The data with no water were taken between these two sets of similar cases. The mean droplet diameter outside the spray is either 41 or 30 microns, for cases 4H, 8SA and 8DA, OS respectively. The 95th percentile diameter is 60 or 44 microns. In both sets, the value with the water flowing is somewhat higher than the cases without the water. This indicates that the measurement locations are either not completely outside the spray or that mist which exists in the exhaust area was being measured. Because the exhaust system did not operate at a consistent value, a change in the background mist from day-to-day is possible. While measurements of the mist are not part of the spray, they also do not really represent noise in the measurement apparatus; they represent something of a bias instead. From these assessments, droplets of 35

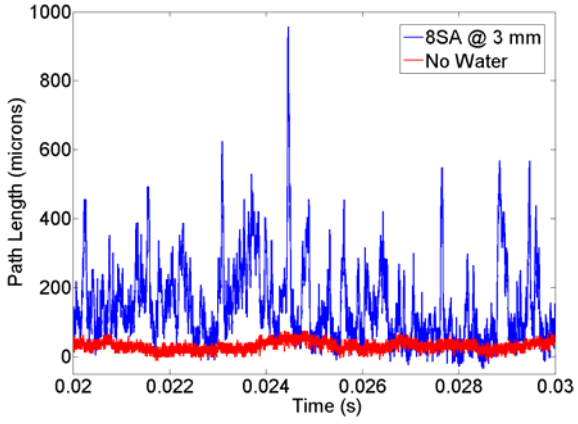

Figure 7: The peaks in the test case with no water are substantially smaller than the peaks when water is flowing; however peaks and troughs still exist.

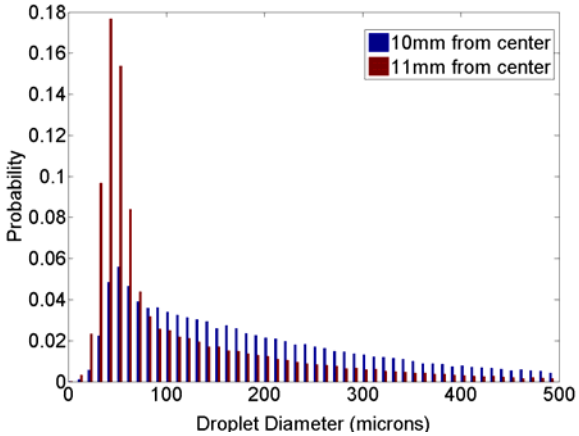

Figure 8: The distribution of droplet diameters changes dramatically at the edge of the spray as shown for case 8SA.

microns and smaller must be viewed skeptically as they are very likely related to noise and not actual resolved droplets. The above appraisal of droplet numbers needed for acceptable statistics was made considering all droplets. If droplets below the threshold value of 35 microns are neglected, the mean generally shifts upward but the other findings change little. For the cases examined here less than 7% of the total droplets measured were below this threshold (across the spray, a greater percentage were below the threshold outside of the spray). In the center of the spray, removing droplets below the threshold diameter increases the mean droplet diameter by 3 to 6%. Ways to lower the system noise and improve signal-to-noise ratio have been identified, and an improved exhaust system is being designed for future use.

In the past, the reported path lengths from x-ray radiography have been time averaged [7-9]. Time-averaged profiles can be generated from the current data by averaging the entire time-resolved signal. The time-averaged path length should be related to the mean droplet diameter, but not identical. (Figure 2 helps to illustrate this point—the mean of the curve is not equal to the maximum value of the curve.) Additionally, in the time-averaged path length, the average includes both the times when no droplets are resolved (at or near zero) and with resolved droplets (well above zero). A typical centerline location has resolved droplets in the beam for approximately 4.6 seconds of the 5 seconds examined. For a single droplet the relationship between averaged path length and the maximum path length depends on the number of measurement points where the droplet was in the beam—the resolution level of the droplet. If the process could pick out a droplet which was in the beam for exactly the measurement time (1 μs here) then the path length maximum would be equal to πD/4, the average chord length of a circle. If the droplet is in the beam for a fraction of the measurement time, this maximum is decreased by the fraction of time spent in the beam because of the data collection process. However, the current post-processing technique cannot detect a droplet unless it has been in the beam about 10 μs. With a resolution level of 10 points or more, the maximum path length is greater than 99% of the droplet's true diameter. The mean path length with this resolution is πD/4. Consequently, if single droplets were being measured and there was always a droplet in the beam the time averaged path length would be π/4 of the mean droplet diameter. The complications of overlapping droplets in the beam and times when no droplets are resolved prevent such a simple conversion from mean path length to droplet diameter. Nevertheless, the qualitative behavior between the two should be similar and will offer some gauge as to whether or not the current technique is trustworthy. Figure 9 shows the mean droplet diameter and the computed, time-averaged path length for the 8SA case at 3 and 5 mm from the injector exit. The qualitative behavior of lobes and asymmetries are comparable for the time-averaged and mean droplet diameters despite the various limitations of the diameter measurement technique as currently applied. Also shown in Fig. 9 is the difference in the mean droplet size caused by neglecting droplets below the threshold value of 35 microns (labeled as "edited" in the figures).

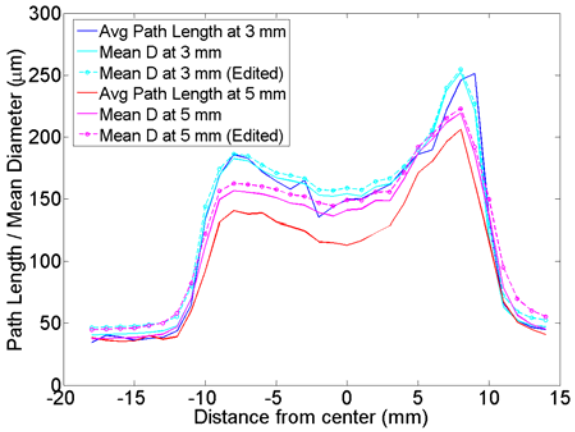

Figure 9: The mean droplet diameter has the same qualitative behavior as the time-averaged path length. Case 8SA is shown.

Figure 10 contains the distribution of droplet diameter at the centerline and at each lobe or "peak" in time averaged path length (+/-7 mm from the center in this example) of case 8DA 5 mm downstream of the injector exit. Each distribution is shown with probability density functions (pdf) overlaid. The pdfs considered were Rosin-Rammler (Weibull) [13] and Log-Normal. Both are calculated including droplets below the threshold value and again neglecting these droplets. Obviously, the Rosin-Rammler function is a poor fit of the current data. Since Rosin-Rammler functions describe many sprays with relative accuracy, why does the current data depart strongly? The pdf somewhat overestimates the width of the diameter distribution and greatly underestimates the probability at the mode. One potential reason is that the current analysis is prone to overestimating droplet diameter, particularly in dense sprays when several droplets could be measured as a single droplet. The Rosin-Rammler function is more sensitive to this type of error than the Log-Normal function. If the distribution is artificially truncated at some upper value, say several hundred microns, the width and probability at the mode predicted by the Rosin-Rammler function improve greatly. At the current time, however, the "true" probability distribution of the spray is unknown, and it is possible that the distribution truly tends to be Log-Normal. The histogram of the velocity distribution, Fig. 11, is also well fit by a Log-Normal pdf. Droplet

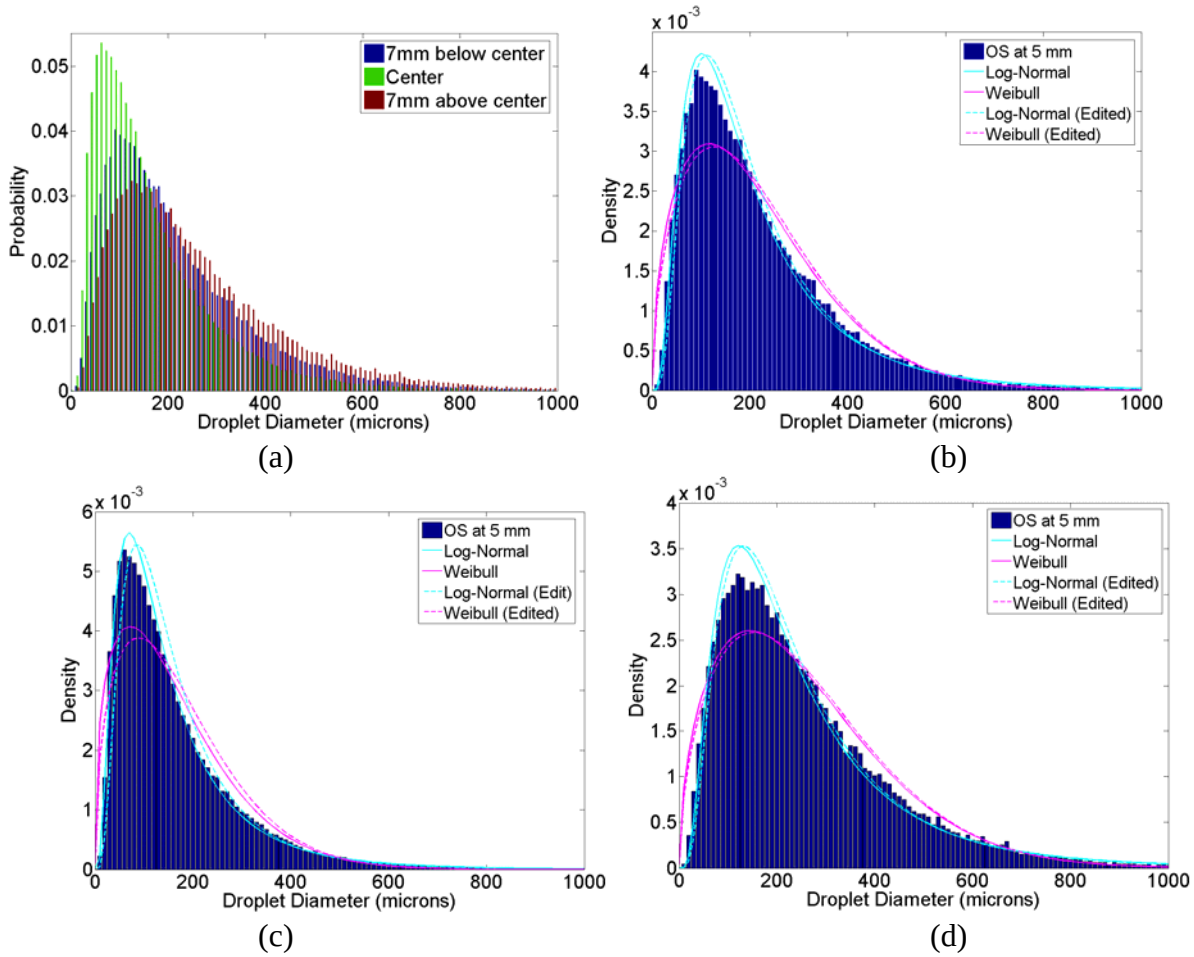

Figure 10: The distribution of droplet diameters differs at the center and the lobes of higher path length found at the edges of the spray. All of the distributions are best represented by a Log-Normal distribution instead of a Rosin-Rammler distribution.

velocities in sprays are known to exhibit Log-Normal distributions, however, so this finding is not surprising. Furthermore, as will be shown below, the droplet velocity measured here is a strong function of the droplet size and its distribution. As a result, a Log-Normal distribution of droplets is prone to produce a Log-Normal distribution of velocities in the current analysis.

Comparing the time-averaged path length (Fig. 9, for example) and the distribution of droplet diameters (Fig. 10, for example), a pattern emerges. The larger the time-averaged path length and median diameter, the wider the droplet diameter distribution. The mode also generally shifts to higher diameters, but the increase in mean diameter is largely due to the widening of the distribution not just this increase in the mode. Previous shadowgraphy studies of GCSC injectors have shown that there are larger droplets in the periphery of the spray with a wider range of sizes than near the center. Similarly, the kurtosis of the distribution decreases at measurement locations with higher mean droplet

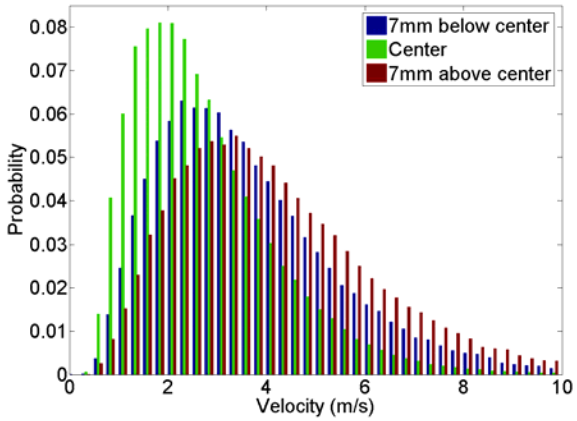

Figure 11: The distribution of velocity, shown here for case 8DA at 5mm downstream, also follows a Log-Normal distribution across various measurement locations within the spray.

diameter. In general, the kurtosis is near 8 in the peak regions of the time-averaged path length and near 12 at the centerline. Both of these values are in substantial excess to the value of 3 for a normal distribution. While the kurtosis increases, the skewness of the diameter distribution is smaller in locations with higher time-averaged path lengths. In all conditions examined and at all locations within the spray skewness is positive and ranges in value from about 1.6 to 2.5. Taken all together, these findings indicate that the increased mean droplet diameter is a result of less small droplets and a wider array of larger droplet diameters and that the edges of the spray have fewer small droplets and more larger droplets than the center.

The distributions of the velocity resemble those for the diameter in many regards (Figs. 10-11). The velocity, then, could be a function of droplet diameter. Given the distributed locations along which droplets are created, the dominant gas momentum and the general sizes of droplets measured, this type of dependence would not be expected. Instead, a dependence would likely be, at least to some extent, an artifact of the limited temporal resolution used in the current set of experiments. Due to the filtering with a running average and limitations in the peak-finding algorithm, droplets are only measured when they are in the line-of-sight of the beam for more than 10 microseconds. The limited resolution, then, sets a maximum droplet velocity which is a function of droplet size, v_{max}=D/10, where D is in microns and the resulting v_{max} is in m/s. So, a 50 micron droplet will not be measured if it is traveling above 5 m/s, but a 500 micron droplet could be traveling 50 m/s and still be resolved. The gas flow for these tests, prior to contact with the liquid, is ~300 m/s. While the gas will slow during expansion and atomization of the liquid, droplets moving in excess of the current limitations would be expected. The limitations explain, in part, the consistent number of droplets found across the spray width despite the increased numbers of droplets likely to pass through a line-of-sight along the spray's diameter (i.e., the spray center) versus a chord near the edge of the spray. Droplets near the injector's axis are likely to be traveling faster than droplets at the spray's periphery. The path-length integrated nature of the measurement results in measurements of the spray's periphery being made at all locations, even the centerline when the beam passes through the periphery, the core and then the periphery again. The current results are limited to slower moving droplets and, therefore, are probably most accurately measuring the peripheries of the spray. While this is certainly a drawback, substantial additional temporal resolution is available at the 7-BM beamline and can be utilized in the future to ease or eliminate the loss of fast-moving droplet data. Furthermore, these are the first quantitative, time-resolved measurements available for dense, GCSC sprays, so even this limited data provides additional insight into the atomization and mixing process.

The droplet's axial velocity limit can be further shown in distributions of velocity as a function of droplet diameter (Fig. 12). An insufficient number of droplets exist at each velocity to provide good statistics, but general trends are visible including a shift to larger mean velocities and a wider range of velocities measured as the droplet diameter increases. Given the velocity dependence on droplet diameter, the best way to compare velocities throughout the spray as the injector is altered is on a droplet-diameter basis. However, this limits the number of droplets considered for velocity comparisons to a few thousand droplets at most, so that general trends and not detailed statistics are available.

The mean velocity as a function of droplet diameter

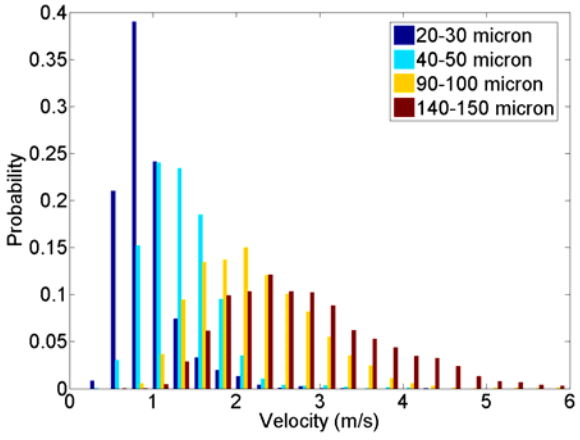

Figure 12: The distribution of velocities for specific droplet diameter ranges (10 microns wide) changes as the diameter increases. Case OS is shown.

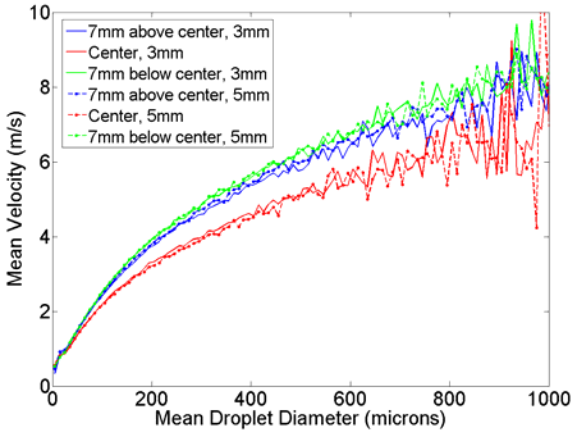

Figure 13: The mean velocity at a given droplet size (10 micron span) increases with the diameter, but not with downstream distance. (OS)

for case OS at the spray centerline and the two areas of peak time-averaged path length is shown in Fig. 13. There is clearly a lower average velocity along the spray's centerline as opposed to the periphery locations (i.e. locations of maximum path length or mean droplet diameter). This deficit is consistent across all operating conditions examined. Given the core gas flow, the velocities at the centerline were expected to increase, not decrease. The truncation of elapsed time when multiple droplets enter the x-ray beam and the expected larger number of droplets across the spray's diameter would likely produce even greater velocities at the centerline. However, more droplets at the centerline are also traveling above the velocity limit for resolution. Also, additional droplets probably lead to more overlapping droplets counted as a single droplet. A bias towards slower velocities could result from these two situations. At present, the anomalous decrease of velocity across the spray center is not understood.

Effect of Geometry Changes in GCSC Injectors

The effect of downstream distance from the injector outlet, outlet diameter, liquid inlet diameter and swirl number of the liquid film on the mean droplet size, distribution and velocity can be examined with this new technique. As with the above assessment of single operating conditions, these comparisons use diameter and its arithmetic mean without using any volume or surface area weighting. Velocity comparisons are made mainly by examining the mean velocity of droplets within 10-micron-sized bins. In other words, the mean velocity of 40 to 50 micron droplets, for example, will be compared between test geometries or locations. It should be noted that in order to maintain a constant momentum flux ratio, the dominant scaling factor for film atomization length, the operating conditions vary somewhat between geometries (Table 1). Further, to maintain good exhaust and minimize splash-back, gas flow rates were limited, so the main difference in operating conditions is the liquid flow rate. Current available test conditions do not allow the impact of these liquid flow rate differences to be measured. Future work will include conditions to investigate whether liquid flow rate has an important effect.

Inside the injector cup, because the liquid flow rates are substantially smaller than the gas flow rates, droplets are expected to accelerate as they move downstream until they achieve the velocity of the gas. For many droplets, this velocity will likely not be achieved within the length of the injector cup. Once outside of the injector, the flow becomes substantially more complex as the spray spreads and entrainment of the outer environment occurs, although these will be minimal at 3 and 5 mm downstream of the injector exit. Secondary breakup is possible throughout the cup and spray. Obviously, the stable upper limit of droplet diameter depends on the gas velocity and, so, the location of the droplet within the spray. Within the core of the spray, though, this value is likely to be at or under 10 microns. In areas outside the core, where entrainment is occurring, the gas velocity is lower, the stable droplet size will be substantially larger and coalescence may occur. Examining the mean droplet diameter, there is a decrease from 3 mm to 5 mm downstream (Fig. 9). The time-averaged path length also decreases. The number of droplets found increases as the spray travels downstream; however, this increase is quite modest—about two to four thousand or about 4% more droplets are found downstream. The skewness and kurtosis of the droplet diameter distributions are similar in both measurement locations. However, there is some increase in the number of smaller droplets and a slight decrease in the number of large droplets downstream which does suggest secondary breakup is occurring. The moderate changes indicate that it is not a strong effect probably because only slow-moving droplets are currently being measured and/or because some amount of coalescence is also occurring. There may be an additional complication, though, which could underestimate the amount of secondary breakup: smaller droplets have shorter time constants, so when accelerating these droplets with smaller diameters would achieve velocities which prevent them from being resolved in a shorter distance than larger droplets. The velocity results suggest that this potential complication is not important in the current set-up. The mean velocity actually decreases in the downstream direction, at direct odds with the expected behavior. Comparing the mean velocities of droplets with similar diameters (Fig. 13) explains the contradiction. There is no appreciable change in the velocity of similar sized droplets over the 2 mm downstream distance. Since there are additional small droplets downstream which result in a lower mean droplet diameter, the overall mean velocity decreases. These findings do not indicate, then, that the spray is slowing. Indeed, given the current limitations in droplet velocity resolution, the likelihood is that the droplet velocity is nearly a constant on the outer periphery where flow entrainment is occurring, since it is hypothesized that this is where the majority of the measured droplets reside.

The liquid inlet diameter should not have an effect on the atomization in a GCSC injector as long as a uniform film is formed prior to atomization. Cases 4H and 8SA (Table 1) have similar total liquid inlet area but either 4 larger or 8 smaller inlets. The swirl levels and liquid mass flow rates are slightly different, but the level of difference is not expected to have any impact on the comparison. The time-averaged path lengths show similar behavior but the asymmetry location is reversed. To compare these two cases, then, one will be "flipped"

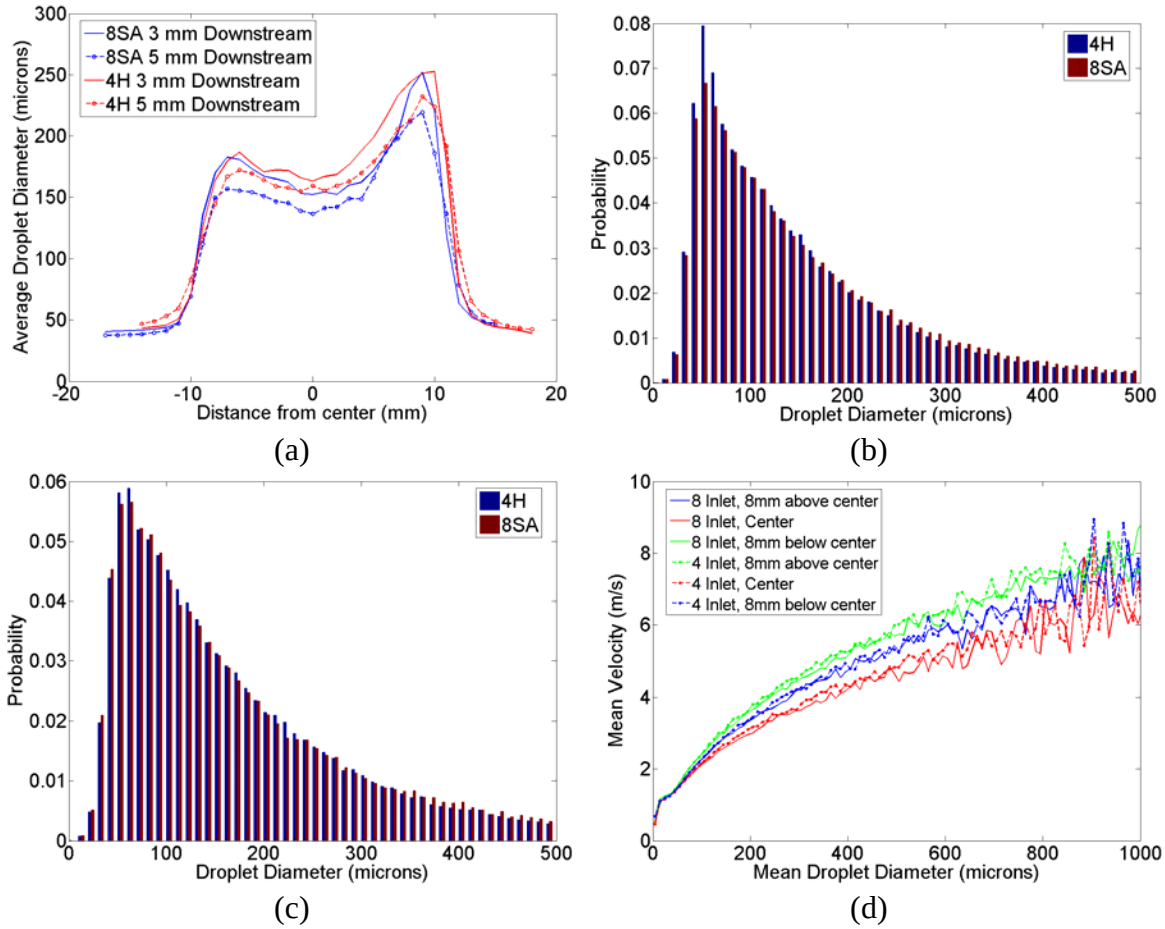

Figure 14: The inlet size impacts the mean droplet diameter (a) but has little effect on the distribution of diameters, for example at the center (b) and 8 mm from the center (c). The mean velocity as a function of droplet diameter also has a slight shift.

about the centerline. The mean droplet diameters also show similar general behavior, but the diameters are larger for the geometry with the larger liquid inlets (Fig. 14a). The overall spray widths are nearly identical, as would be expected. Larger droplet diameters could result from larger wall-bound structures that have additional surface area. Coherent structures have been visualized in similar injectors without a sheltered area for liquid development [4]. However, earlier visualizations in the injector cup of the exact geometries under study [2], showed that the initial shelter between the gas and liquid fully fills with water creating a uniform film before the initial liquid-gas contact. The results seem to suggest some "memory" of the inlet conditions which impacts the size the atomizing structures despite the atomization being driven by the gas-phase flow. However, given later-discussed comparisons with lower swirl levels, the slightly altered swirl cannot be fully ruled out as the cause. The droplet diameter distributions suggest similar atomization and secondary breakup behavior for the two inlet diameters—the general characters of the two are nearly identical despite the difference in mean (Figs. 14b & c). This similarity is at odds with the findings for swirl's effect and, so, again suggests "memory" of the inlet and not swirl is the cause of the observed changes. Along with the difference in droplet diameter, there is a slight difference in the mean velocity as a function of droplet diameter. The velocities are slightly larger for the larger liquid inlet (Fig. 14d). The gas flow rates are identical and the liquid flow rate is actually larger for the smaller inlets, so the reason for the larger velocity is not clear at this time.

The different liquid inlets, discussed above, have similar total areas so that the swirl number of the incoming liquid is nearly identical. Case 8DA (Table 1) has twice the total inlet area and, hence, a lower swirl number. Each of the 8 inlets in case 8DA are the diameter of the 4 inlets in case 4H. Lower swirl should produce a spray with less tangential velocity at the injector outlet. Previous studies inside the injector cup show similar film lengths suggesting swirl is a secondary effect in the atomization of these injectors

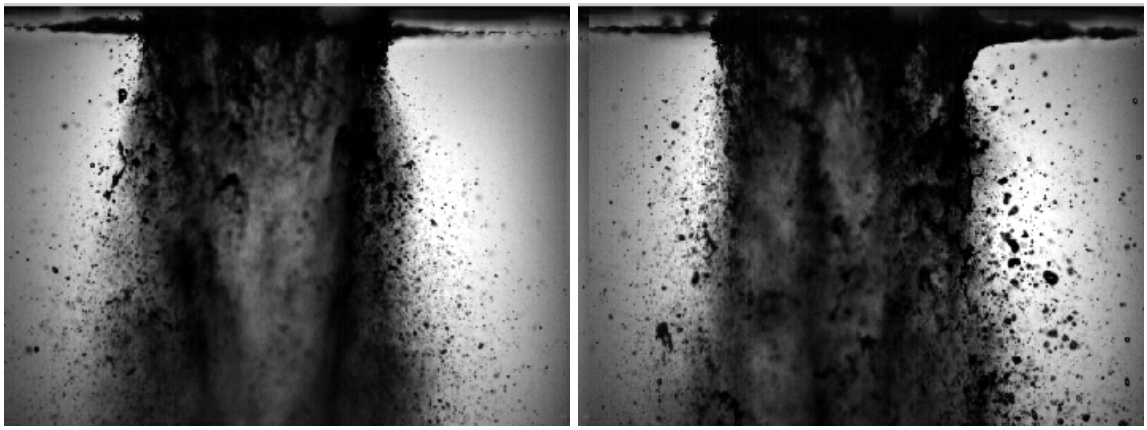

Figure 15: Shadowgraphs show larger droplets on the periphery of sprays with less swirl (right).

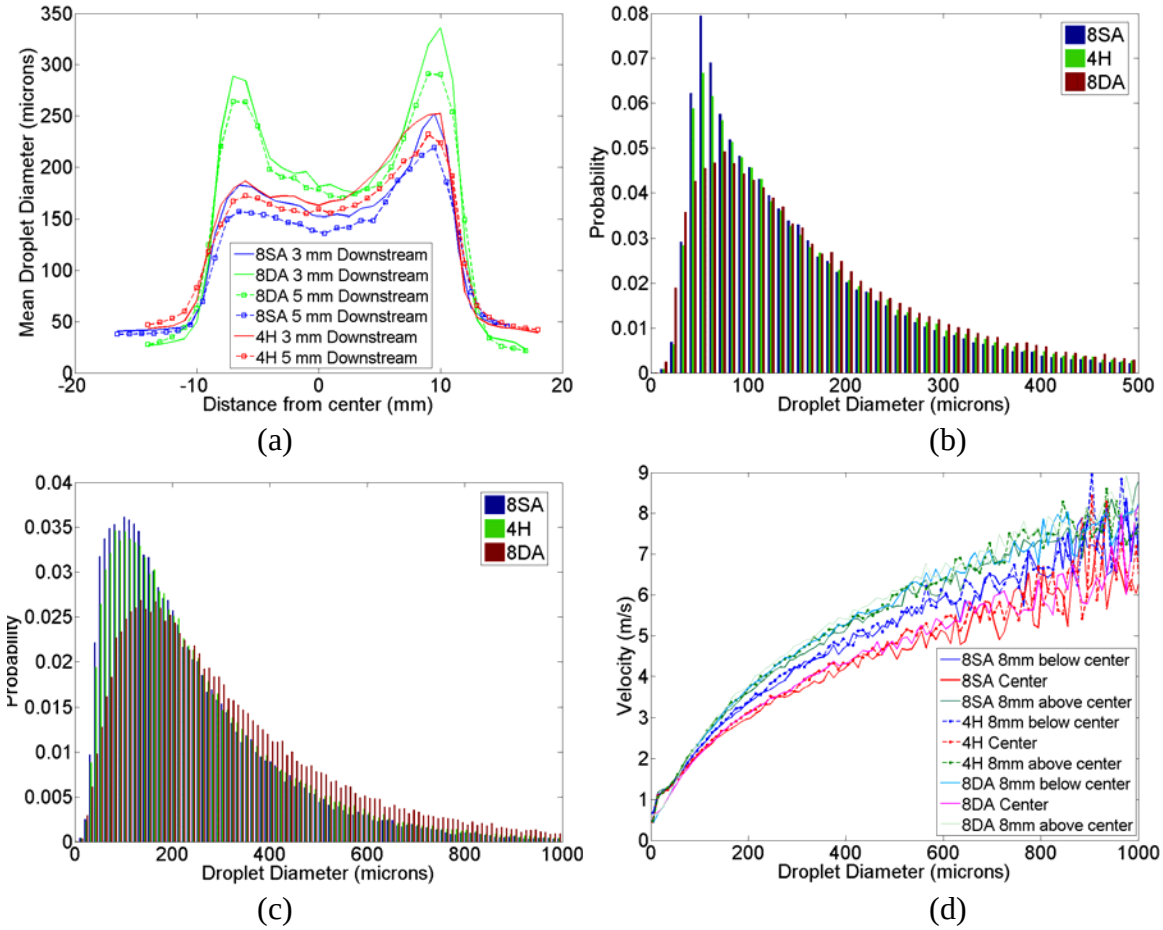

Figure 16: The mean diameter (a) and the diameter distribution (at the center, b, and 8 mm above the center, c) are altered by the swirl. The mean velocity as a function of droplet diameter also changes with swirl level.

[2]. However, shadowgraphy of the injectors shows larger droplets on the periphery of the lower swirl number injector (Fig. 15) suggesting a difference in behavior after primary atomization. In the current study, the mean droplet diameter is indeed larger for the lower swirl number case compared to either of the higher swirl cases, matching either inlet number or inlet diameter (Fig. 16a). The lower swirl number case is also wider than the higher swirl cases in contradiction to the expected detriment in tangential velocity at the exit. This finding seems to suggest that the droplets maintain very little tangential velocity and the gas picks up little or no tangential component from the swirling liquid at the conditions investigated. One way in which

tangential velocity could be lost from the droplets is if they strike the injector wall and reatomize. The more tangential velocity the droplets originally have, the more this process would occur which could lead to smaller droplets due to reatomization, less coalescence due to less mass at the injector core and greater loss of both tangential and axial velocity. The lower the swirl number, the wider and more distributed the droplet diameters are (Fig. 16b): the lower swirl number case has less excess kurtosis. In the location where the higher swirl number geometries have large asymmetries, the droplet diameter distribution is much narrower and also more skewed towards smaller droplet diameters (Fig. 16c). Unlike changes in inlet size alone, changes in swirl number appear to impact the basic atomization mechanisms at work in producing and or evolving the spray. The mean velocity as a function of droplet size is larger for the lower swirl number, especially if the number of inlets is matched. The difference is particularly severe in the location of the asymmetry in the lower swirl number geometries (Fig. 16d). The change in droplet velocities lends some support to the idea that droplets depositing on and reatomizing from the walls could be the source of seemingly anomalous mean droplet diameter behavior. Currently, however, no independent or additional evidence exists for this mechanism and the current limitations in the diagnostic may still be responsible for some of the observed differences.

The outlet diameter is expected to have little impact on droplet diameter beyond those expected from a slightly increased gas velocity (in terms of droplet acceleration and secondary breakup) assuming that the momentum flux ratio is held constant. Figure 17a shows that the spray from a narrower injector (OS) is indeed narrower (than 4H), but also shows a slight increase in droplet diameter. The increase could be a direct result of the faster gas velocity accelerating smaller droplets to a point beyond which they can be resolved. If this biasing is taking place, then the mean velocity at a given droplet diameter should be larger for the narrower outlet. There is a slight increase in this

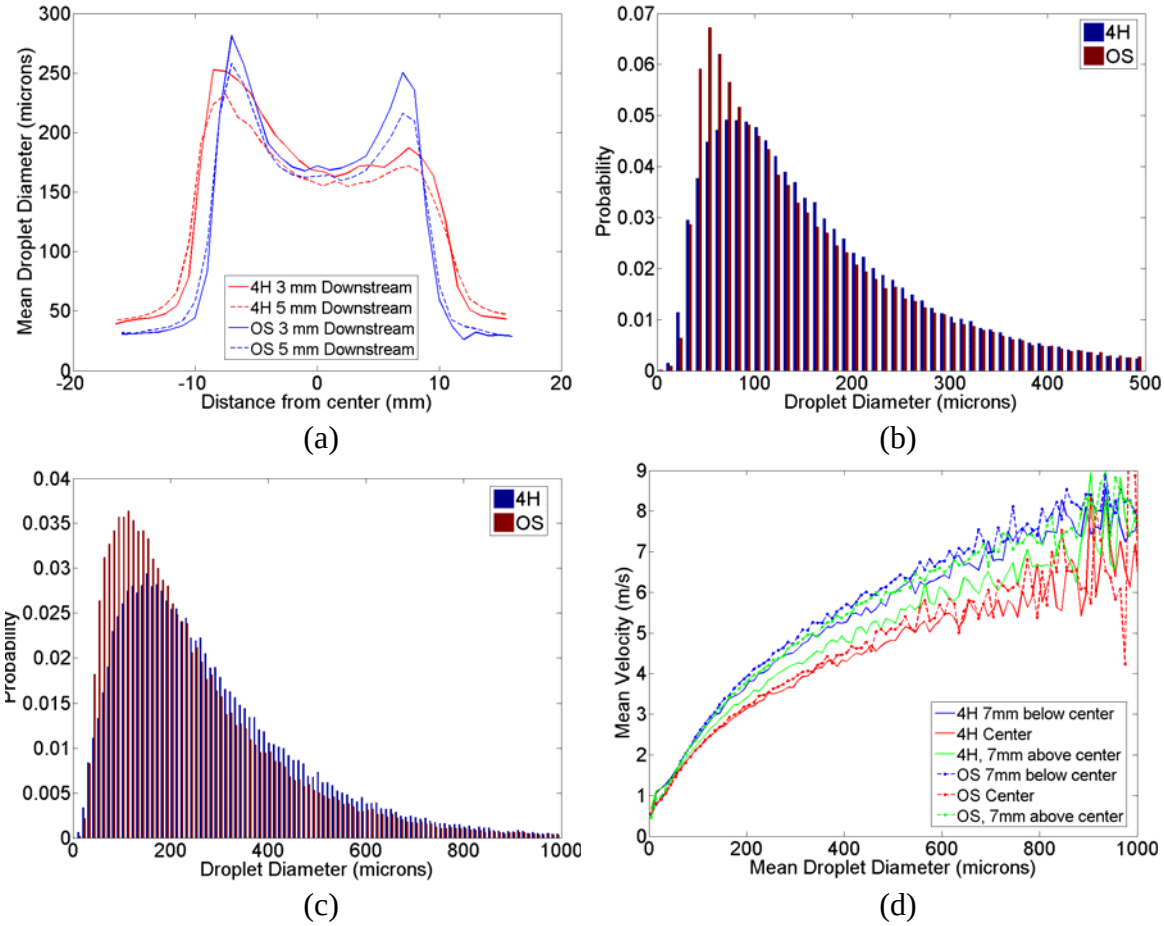

Figure 17: The outlet size has a small impact on the mean droplet diameter (a); however, the spray clearly narrows and the asymmetries are different. There is some change in distribution at the center (b), but mostly the character is similar with the mean just shifted higher, like at 7mm from center (c). The mean velocity is similar except where the asymmetries are very different (7 mm above the center).

mean velocity, but it is only very evident in the location where the wider spray (4H) has a lower droplet diameter due to asymmetries (Fig. 17d). The asymmetry complicates the comparisons because the flow process in that location may be very different between the two outlets. Overall, then, it is unclear if the biasing due to droplet acceleration is really occurring or if there is a true increase in droplet diameter with the smaller diameter injector outlet. The droplet diameter distributions (Fig. 17b & c) also hint that acceleration of small droplets may be the cause of increased mean diameter. The distributions' shapes are similar in the center and at the location of maximum mean diameter, but the narrower outlet geometry is shifted to slightly larger diameters. The same general character may indicate similar atomization processes.

Conclusions

The use of x-ray radiography to measure time-resolved spray statistics such as droplet diameter has been detailed for a Gas-Centered Swirl Coaxial injector. In typical operation these injectors produce an optically dense spray that prevents quantitative interrogation by visible-light diagnostics. The measurements here, then, represent the first quantitative, time-resolved measurements in these sprays. The basic performance of the diagnostic, measurements from four different sprays and the effect of downstream location, inlet size, swirl number (inlet area) and outlet diameter were all examined.

The current results were not the main focus of the testing campaign and certain decisions limited the performance of the time-resolved diagnostic. Nevertheless, the mean droplet diameters follow the same trends as the time-averaged path lengths indicating that the basic, underlying behavior and changes are being recorded. Analysis of the convergence of the mean diameters indicated that tens of thousands of droplets were necessary to achieve good statistics. Droplet diameter distributions were more of a Log-Normal profile than that predicted by a Rosin-Rammler fit. The distributions may be skewed by the 1 MHz sampling rate and the post-processing of the data. These set a minimum time over which a droplet had to remain in the beam in order to be measured and, as a result, a maximum droplet velocity. Distributions of droplet velocity as a function of droplet diameter indicated clipping was occurring. The clipping may bias the results towards larger droplets and those at the peripheries of the spray. The 7-BM beamline is capable of achieving substantially increased sampling rates; increased rates will be used in future testing to reduce the current limitations.

Some comparisons were made between axial locations in the spray and geometries of the GCSC injectors. At downstream locations the number of droplets increased modestly and the mean droplet diameter decreased indicating secondary breakup was occurring. No increase in mean velocity as a function of droplet size was observed, however. The lack of increase in velocity suggests that the measurements may currently be biased towards the outer periphery of the spray. Despite expectation, the liquid inlet diameter was seen to impact the size and velocity of the droplets. Because the initial shelter fully fills with liquid and a film is formed prior to contact with the gas, the spray was expected to have no "memory" of the liquid inlet. The overall droplet size distributions were similar between the inlets suggestive of similar atomization behaviors and spray evolution, but the mean droplet diameters were about 15% higher at the centerline when the inlet diameter was doubled (and the overall inlet area kept the same). A decrease in injector outlet diameter also increased the droplet size while the distribution of droplet diameters remained similar. In the case of the increased outlet diameter, however, the shift to larger diameters may be an artifact of higher gas velocities and the limit velocity resolution of the current set-up. The changes in the spray as the swirl was altered (through changes in liquid inlet area) were unexpected but agreed with qualitative shadowgraphs. A lower swirl number increased the spray width and increased the mean droplet diameter despite similar primary atomization behavior. The mean velocity as a function of droplet diameter also increased despite similar gas velocities. In the case of altered swirl, the distribution of droplet diameters also changed substantially indicating that differences in behavior, which have not yet been observed, are likely causing different spray evolution as the swirl number is altered.

Overall, the current work produced an initial investigation into the utility of time-resolved x-ray radiography for producing droplet statistics. Additional insight into GCSC sprays was developed. Several improvements to the technique, which are easily implemented, were identified and will be used in future efforts. These include calibration of the technique and implementation of a process to deconvolve multiple droplets within the beam; moving to a lower energy level of the x-rays to improve the signal-to-noise ratio; and increasing sampling rates to enhance velocity and droplet resolution in future testing. Improvements in the exhaust system will also be made.

Acknowledgements

A portion of this research was performed at the 7-BM beamline of the Advanced Photon Source, Argonne National Laboratory. Use of the Advanced Photon Source was supported by the U.S. Department of Energy, Office of Science, Office of Basic Energy Sciences, under Contract No. DE-AC02-06CH11357. Daniel Duke (Monash University), Chad Eberhart

(University of Alabama, Huntsville), Benjamin Halls (Iowa State University), William Miller (Kettering University) and Christopher Powell (Argonne National Laboratory) assisted in the conduction of the experiments enabling the collection of data the beyond the initial scope of investigation.

References

1. Sutton, G.P., *History of Liquid Propellant Rocket Engines*, AIAA, 2006.
2. Schumaker, S.A., Danczyk, S.A. and Lightfoot, M.D.A., *47th AIAA Joint Propulsion Conference*, San Diego, CA, July 2011,
3. Lightfoot, M.D.A., Schumaker, S.A., Villasmil, L.A. and Danczyk, S.A., *JANNAF 8th Modeling and Simulation, 6th Liquid Propulsion, and 5th Spacecraft Propulsion Joint Subcommittee Meeting*, Huntsville, AL, December 2011,
4. Schmidt, J.B., Schaefer, Z.D., Meyer, T.R., Roy, S., Danczyk, S.A. and Gord, J.R., *Applied Optics* 48 (4):B137-B144 (2009).
5. Strakey, P.A., Talley, D.G. and Hutt, J.J., *Journal of Propulsion and Power* 17 (2):404-410 (2001).
6. Heindel, T.J., *Journal of Fluids Engineering* 133 (7):074001 (2011).
7. Lin, K.C., Carter, C., Smith, S. and Kastengren, A.L., *50th AIAA Aerospace Sciences Meeting*, Nashville, TN, January 2012, AIAA 2012-0347.
8. Halls, B.R., Heindel, T.J., Meyer, T.R. and Kastengren, A.L., *50th AIAA Aerospace Sciences Meeting*, Nashville, TN, January 2012,
9. Kastengren, A.L., Powell, C.F., Liu, Z., Moon, S., Gao, J., Zhang, X. and Wang, J., *22nd Annual Conference on Liquid Atomization and Spray Systems*, Cincinnati, OH, May 2010,
10. Leick, P., Kastengren, A.L., Liu, Z., Wang, J. and Powell, C.F., *11th Triennial International Conference on Liquid Atomization and Spray Systems*, Vail, CO, May 2009,
11. Kastengren, A.L., Powell, C.F., Arms, D., Dufresne, E.M. and Wang, J., *22nd Annual Conference on Liquid Atomization and Spray Systems*, Cincinnati, OH, May 2010,
12. Berger, M.J., Hubbell, J.H., Seltzer, S.M., Chang, J., J.S., C., Sukumar, R., Zucker, D.S. and Olsen, K., *XCOM: Photon Cross Sections Database, NIST Standard Reference Database 8 (XGAM)*, http://www.nist.gov/pml/data/xcom/index.cfm. , 2012.
13. R2008b, M., MathWorks Inc., 2008.